Improved Multiscale Permutation Entropy for Biomedical Signal Analysis: Interpretation and Application to Electroencephalogram Recordings

Improved Multiscale Permutation Entropy for Biomedical Signal Analysis: Interpretation and Application to Electroencephalogram Recordings

Hamed Azami[1] and Javier Escudero[2]

[1,2]*Institute for Digital Communications, School of Engineering, University of Edinburgh, Edinburgh, King's Buildings, EH9 3JL, UK*

Emails: [1]hamed.azami@ed.ac.uk; [2]javier.escudero@ed.ac.uk

Abstract: Permutation entropy (PE) is a well-known and fast method extensively used in many physiological signal processing applications to measure the irregularity of time series. Multiscale PE (MPE) is based on assessing the PE for a number of coarse-grained sequences representing temporal scales. However, the stability of the conventional MPE may be compromised for short time series. Here, we propose an improved MPE (IMPE) to reduce the variability of entropy measures over long temporal scales, leading to more reliable and stable results. We gain insight into the dependency of MPE and IMPE on several straightforward signal processing concepts which appear in biomedical activity via a set of synthetic signals. We also apply these techniques to real biomedical signals via publicly available electroencephalogram (EEG) recordings acquired with eyes open and closed and to ictal and non-ictal intracranial EEGs. We conclude that IMPE improves the reliability of the entropy estimations in comparison with the traditional MPE and that it is a promising technique to characterize physiological changes affecting several temporal scales. We provide the source codes of IMPE and the synthetic data in the public domain.

Keywords: Multiscale permutation entropy, biomedical signal analysis, electroencephalogram, non-linear analysis, signal regularity, complexity.

1. Introduction

There are several main types of measures, such as, entropies and fractal dimensions, to compute the complexity of a system or signal. These are used to compare signals and distinguish or detect regular and random epochs (Bandt and Pompe 2002). As mentioned in (Kantz, Kurths et al. 2011), healthy subjects and people with disease can often be distinguished by the complexity of their physiological activity (Goldberger, Peng et al. 2002).

Entropy is one of the most popular and powerful concepts to evaluate the dynamical characteristics of a signal. This metric measures the uncertainty and irregularity of a time series. Higher entropy generally demonstrates higher uncertainty, whereas lower entropy shows more regularity and certainty of a system (Bandt and Pompe 2002, Sanei 2013). There are a number of entropy approaches commonly applied to physiological recordings, such as approximate entropy (ApEn) (Pincus 1991), sample entropy (SaEn) (Richman and Moorman 2000), fuzzy entropy (FuEn) (Chen, Wang et al. 2007), permutation entropy (PE) (Bandt and Pompe 2002) and wavelet entropy (Rosso, Blanco et al. 2001), each of which has its own advantages and disadvantages (Holzinger, Hörtenhuber et al. 2014).

PE is based on the order relations among values of a signal, the permutation patterns. It is analogous to the Lyapunov exponents for some well-known chaotic dynamical systems, such as the noise-free logistic map, although PE yields more meaningful results in the presence of

observational and dynamical noise (Bandt and Pompe 2002, Zanin, Zunino et al. 2012). Compared with the other entropies, such as ApEn and FuEn, PE is theoretically simple and it has fewer parameters, it is relatively robust to artifacts and noise, and is computationally fast. Furthermore, the PE can be used for both the non-stationary and nonlinear signals. With respect to the signal length, PE is more robust than the zero-crossing rate (ZCR) (Bandt and Pompe 2002). Because of the aforementioned advantages, PE has been extensively employed in the numerous real world physiological signal and image processing applications (Morabito, Labate et al. 2012, Zanin, Zunino et al. 2012). For example, Li et al. investigated the behaviour of PE to predict absence seizures in rats using EEG signals (Li, Ouyang et al. 2007). They showed that PE can track the dynamical changes of EEG recordings and that PE can predict absence seizures better than SaEn (Li, Ouyang et al. 2007). Ferlazzo et al. employed PE to reveal abnormalities of cerebral activity in patients with typical absences (Ferlazzo, Mammone et al. 2014). They concluded that PE is a valuable tool to detect abnormalities of cerebral electrical activity which are not revealed by conventional approaches for EEG signals (Ferlazzo, Mammone et al. 2014).

However, PE is limited to assessing the values of entropy for only one temporal scale, the one associated with the original sampling of the signals. This may limit the ability of PE to inspect dynamics residing at longer temporal scales. In this sense, multiscale entropy (MSE), proposed by Costa et al. (Costa, Goldberger et al. 2002), calculates entropy over a range of scales to evaluate the complexity of a time series. In the original definition of MSE, SaEn was the metric used to assess the entropy over the temporal scales (Costa, Goldberger et al. 2002). Nonetheless, the concept of multiscale evaluation of entropy can be extended to other entropy metrics. Morabito et al. used multiscale PE (MPE) to assess the complexity of electroencephalogram (EEG) recordings in Alzheimer's disease (Morabito, Labate et al. 2012).

The multiscale evaluation of entropy has notorious advantages. First of all, it allows us to inspect dynamics along more than one temporal scale. This is very significant for biological systems which need to operate across multiple spatial and temporal scales, and therefore their complexity is also multiscaled (Costa, Goldberger et al. 2005). Secondly, unlike SaEn, MSE is consistent with the Fogedby study (Fogedby 1992) illustrating that the complexity of 1/*f* noise is higher than white Gaussian noise (WGN).

The coarse-graining of MPE and MSE methods are based on Costa's algorithm (Costa, Goldberger et al. 2002, Morabito, Labate et al. 2012). The first step of MPE, the coarse-graining process, considerably reduces the time series length because, to inspect the deeper temporal scales, MPE uses a procedure similar to sub-sampling. This may yield an imprecise estimation of entropy when the time series is too short. Hence, the basic MPE method may not provide a reliable analysis for short time series. To overcome this problem, in this paper, an improved MPE (IMPE) is proposed. This is in contrast with the alternative MPE algorithm by (Shaobo, Kehui et al. 2014) called modified MPE (MMPE). In the MMPE, a coarse-grained sequence is built subsampling the original signal by taking one out of τ samples, where τ denotes the temporal scale. However, no filtering is used. Therefore, this procedure will necessarily lead to aliasing, thus changing important properties of the signal. For example, for $\tau = 3$ and *i*=2, $\mathbf{y}^{(3)}(2, j) = \{x_2, x_5, x_8, ...\}$, some important information of the original time series $\{x_1, x_2, ..., x_N\}$ may be omitted in the MMPE.

Because of the relevance and the possible usefulness of MPE and IMPE in a number of biomedical signal analyses, it is important to understand and exemplify the behavior of the measure for different kinds of classical signal concepts such as frequency, amplitude, noise

power, and signal bandwidth. This study addressed this issue to help to illustrate the dependency of both MPE and IMPE on these concepts and to compare both techniques. Moreover, we will illustrate the application of MPE and IMPE to five different datasets of real EEG signals.

In the following section, the concepts of PE and MPE are described. Our proposed method is explained in Section 3. In Section 4, the synthetic signals and real EEG datasets employed in this paper are introduced. Then, the results and discussions of the proposed method (IMPE) and the conventional MPE are explained in Sections 5 and 6, respectively. The conclusions of the paper are drawn in the last section.

2. Background on PE and MPE

In this section, we briefly describe PE and MPE.

2.1. Permutation Entropy

Assume we have a given time series of length N, and let the time series be $\mathbf{y}=\{y_1, y_2, ..., y_N\}$. At each time t of $\mathbf{y}$, a vector including the d-th subsequent values is constructed as: $\mathrm{Y}_t^{d,l}=\{y_t, y_{t+l}, ..., y_{t+(d-2)l}, y_{t+(d-1)l}\}$ for t=1,2,…,N-(d-1)l, where d, which is named the embedding dimension, determines how much information is contained in each vector and l is the time delay. To calculate the PE, the d values y_i are associated with numbers from 1 to d and arranged in increasing order as $\{y_{t+(j_1-1)l}, y_{t+(j_2-1)l}, ..., y_{t+(j_{d-1}-1)l}, y_{t+(j_d-1)l}\}$. For different samples, there will be d! potential ordinal patterns, π, which are named "motifs". For each π_t, $p(\pi_t)$ demonstrates the relative frequency as follows:

$$p(\pi_i^{d,l}) = \frac{\#\{t | t \le N-d, \text{type}(\mathrm{Y}_t^{d,l}) = \pi_i^{d,l}\}}{N-d+1} \tag{1}$$

where #{} denotes the cardinality of the set (the number of elements) (Bandt and Pompe 2002, Zanin, Zunino et al. 2012). The PE is computed as follows:

$$H(\mathbf{y}, d, l) = -\sum_{\pi_k=1}^{\pi_k=d!} p(\pi_k) \ln p(\pi_k) \tag{2}$$

When all motifs have equal probability, the largest value of PE is obtained, which has a value of $\ln(d!)$. In contrast, if there is only one $p(\pi_k)$ different from zero, which illustrates a completely regular signal, the smallest value of PE is obtained as much as 0 (Bandt and Pompe 2002, Zanin, Zunino et al. 2012).

2.2. Multiscale Permutation Entropy

MPE, like MSE, includes two main steps. First, a "coarse-graining" process is applied to a time series. Consider a real-valued time series $\{x_1, x_2, \cdots, x_N\}$ of length *N*. Multiple successive coarse-grained versions are made by averaging the time data points within non-overlapping windows of increasing length τ, which is called scale factor. A schematic illustration of the coarse-grained procedure is shown in Figure 1. According to the following equation, each element of the coarse-grained time series $\mathbf{y}_j^{(\tau)}$ is defined as:

$$\mathbf{y}_j^{(\tau)} = \frac{1}{\tau} \sum_{i=(j-1)\tau+1}^{j\tau} x_i \qquad 1 \le j \le \left\lfloor \frac{N}{\tau} \right\rfloor \tag{3}$$

where $\lfloor a \rfloor$ denotes the largest integer not greater than a. The length of each coarse-grained time series is $\left\lfloor \frac{N}{\tau} \right\rfloor$. Second step is calculating the PE for each coarse-grained time series. The attained values can be plotted as a function of the scale factor τ (Costa, Goldberger et al. 2002, Morabito, Labate et al. 2012).

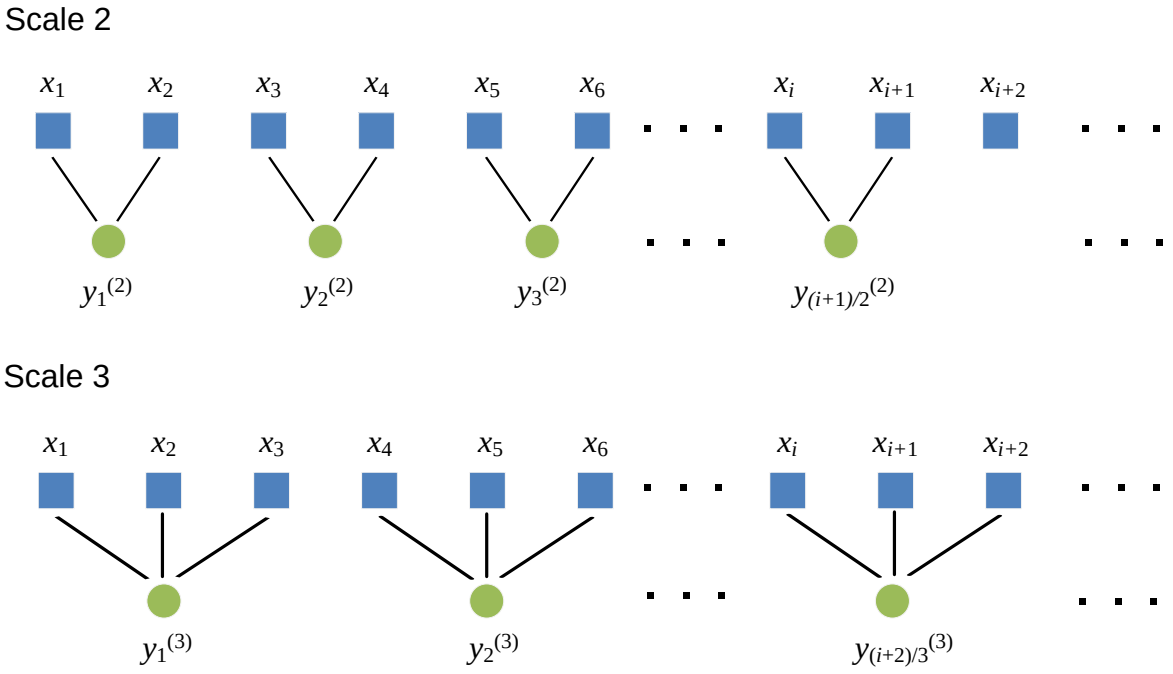

Figure 1. The scheme demonstrating the coarse-graining of a sequence for scale factor $\tau = 2$ and $\tau = 3$. Figure is modified from the one published in (Costa, Goldberger et al. 2005).

3. Improved Multiscale Permutation Entropy

The conventional MPE has two main drawbacks. Firstly, the MPE is not symmetric. For example in scale 3, we could rationally expect the metric to behave the same for x_3 and x_4, in comparison with x_2 and x_3. However, at scale 3, x_1, x_2 and x_3 are separated from x_4, x_5 and x_6. The second drawback is the relative variability of the MPE results for long temporal scales. When the MPE

is computed, in the coarse-graining process, the number of samples of the resulting coarse-grained sequence is $\left\lfloor \frac{N}{\tau} \right\rfloor$. When the scale factor τ is high, the number of samples in the coarse-grained sequence decreases. This may yield an unstable measure of entropy.

To overcome these problems, the IMPE is proposed based on the idea originally reported by Wu for MSE (Wu, Wu et al. 2014). Here, because of some advantages of PE over SaEn, we use PE instead. Hence, the IMPE is calculated in two main steps:

1) In the first step, $z_i^{(\tau)} = \{y_{i,1}{}^{(\tau)}, y_{i,2}{}^{(\tau)}, ...\}$ are generated where $y_{i,j}{}^{(\tau)} = \frac{\sum_{f=0}^{\tau-1} x_{f+i+\tau(j-1)}}{\tau}$. As can be observed in Figure 2, in the IMPE algorithm, for each τ, we have τ different time series $z_i^{(\tau)} \mid (i = 1, ..., \tau)$, while in the MPE method, only $z_1^{(\tau)}$ is considered.

2) For a defined scale factor τ and embedding dimension *d*, PE of each of $z_i^{(\tau)} \mid (i = 1, ..., \tau)$ is separately calculated. Then, the average of PE values is computed as follows:

$$\mathrm{IMPE}(x, \tau, d) = \frac{1}{\tau} \sum_{i=1}^{\tau} \mathrm{PE}(z_i^{(\tau)}) \tag{4}$$

d determines the number of accessible states *d*! .

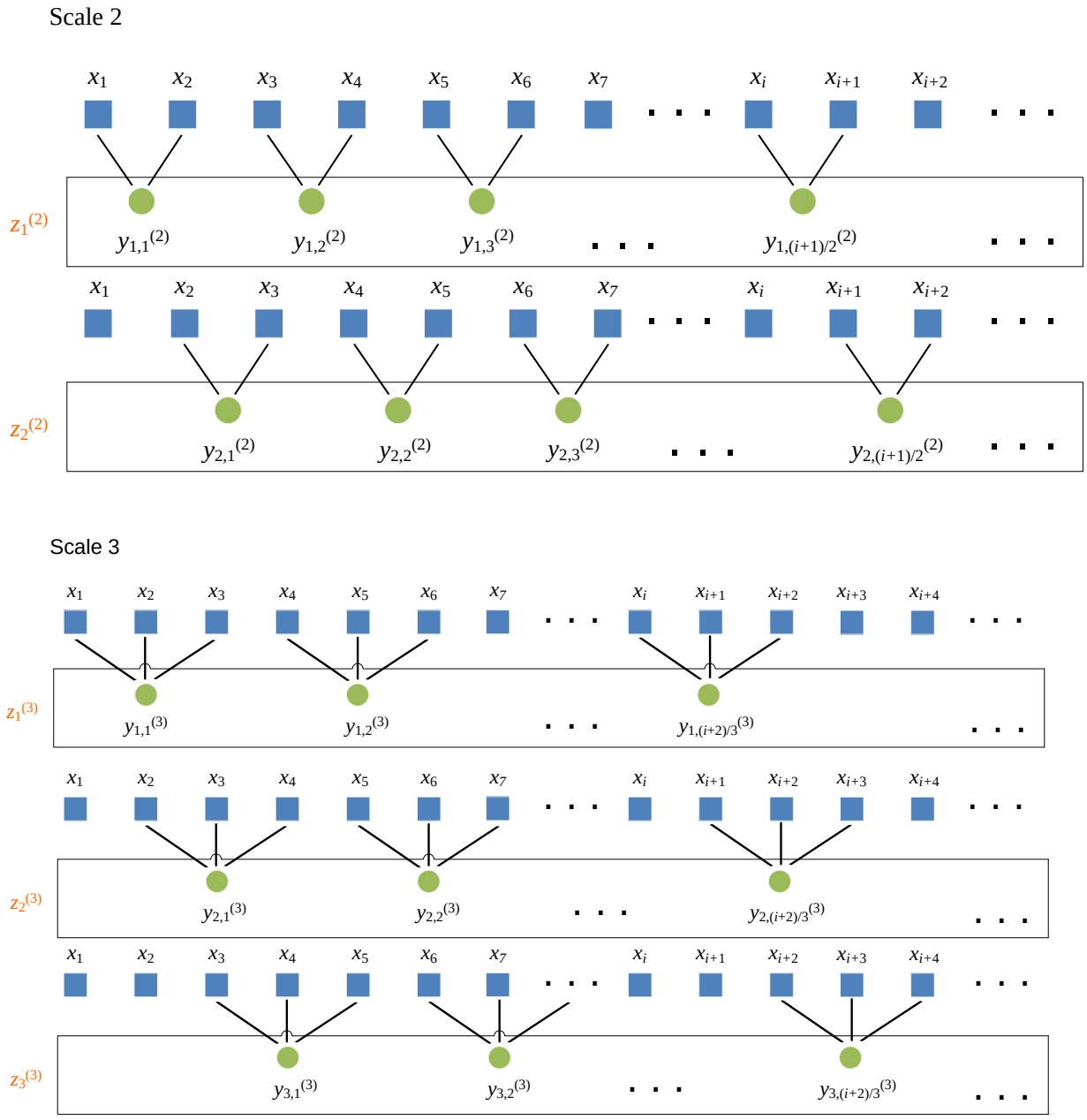

Figure 2. The scheme demonstrating the proposed coarse-graining of a sequence for scale factor $\tau = 2$ and $\tau = 3$.

Due to the key role of embedding dimension for the PE, an important issue is choosing the embedding dimension *d*. In order to work with reliable statistics, for calculating PE, it is highly recommended $d! \ll N$ or $(d+1)! \leq N$ (Kowalski, Martín et al. 2007, Li, Yan et al. 2014). In addition, when *d* is too large, the computation time will be higher. On the other hand, when *d* is high, the number of accessible states will be large, and the value of the PE will probably be more reliable. All in all, we should make a trade-off between the aforementioned cases. It is worth noting that, since the number of sample points for a coarse-grained sequence at level τ is $\left\lfloor \frac{N}{\tau} \right\rfloor$, we have the condition $(d+1)! \leq \left\lfloor \frac{N}{\tau} \right\rfloor$ for MPE or IMPE.

4. Evaluation signals

To evaluate the IMPE and MPE, we will use both synthetic signals and real EEG data.

4.1. Synthetic signals

In this subsection, the signals used to study the MPE and IMPE measures, and their interpretability in terms of classical signal processing concepts such as frequency, amplitude, noise power, and signal bandwidth are described. We also consider the performance of the entropy metrics on WGN and 1/*f* noise. All these synthetic signals, except WGN and 1/*f* noise, have a sampling frequency (f_s) of 150 Hz and a length of 100 s. Therefore, they have 15000 sample points. The time plots of these synthetic signals, and their corresponding spectrograms, and two zooms (for each kind of signal) on their start and end, to demonstrate the changes in their characteristics, appear in Figure 3. Some of them have been employed to inspect the Lempel-Ziv complexity measure and auto-mutual information function rate of decrease and have been explained in (Aboy, Hornero et al. 2006) and (Escudero, Hornero et al. 2009) respectively.

1) MPE and IMPE Versus Noise Signals**:** White Gaussian noise is a random signal which has equal energy across all frequencies. The name white originates from the fact that this kind of signal has a constant power spectral density $S(f)$ as follows:

$$S(f) = \frac{C_w}{|f|^0} \tag{5}$$

where C_w is a constant (Sejdić and Lipsitz 2013). White can be regarded as a sequence of consecutively uncorrelated random variables with zero mean and finite variance (Diebold 2006). A stochastic process appropriate to model evolutionary or developmental systems characterized by equal energy per octave is called pink noise, whose power spectral density is as follows:

$$S(f) = \frac{C_f}{|f|^\alpha} \tag{6}$$

where C_f is a constant and α can be changed between 0 and 2. As can be seen in Equation 6, the power spectrum density of pink noise is inversely proportional to frequency (Sejdić and Lipsitz 2013). We expect pink noise to be more complex than WGN, due to the presence of long-range correlations in the data.

2) MPE and IMPE Versus Frequency: In order to clarify how the MPE and IMPE change when the amplitude and frequency of sinusoidal signals are changed, two kinds of synthetic signals are created. The first one consists in a constant amplitude chirp signal whose frequency is swept logarithmically from 0.1 Hz to 30 Hz in 100 s. The second kind of signal, whose frequency is swept logarithmically from 0.25 Hz to 5 Hz in 100 s, was generated by modulating the amplitude of the chirp signal by a pure sinusoid. MPE and IMPE were applied to each of the two kinds of signals using a moving window of 6.667 s with 80% overlap with the objective of testing if MPE

and IMPE are sensitive to frequency or amplitude changes. Figures 3(a) and 3(b) demonstrate the constant chirp signal and the amplitude modulated chirp, respectively.

3) MPE and IMPE Versus Noise Power: In order to understand how the MPE and IMPE change with the level of noise affecting quasi-periodic signals, we created an amplitude-modulated quasi-periodic signal with additive WGN of diverse power. The signal was generated as an amplitude-modulated sum of two sine waves with frequencies at 0.5 Hz and 1 Hz. The first 20 s of this sequence does not have any noise. After that, WGN was added to the signal, with the noise power increasing every 10 s. Figure 3(c) shows this time series.

4) MPE and IMPE Versus Bandwidth of Colored Noise: In order to determine the relationship between MPE or IMPE and noise bandwidth, a synthetic signal consisted of a 100-s time series composed of the five segments of colored noise with increasing bandwidth is employed. The frequency spectra of the colored noises are all centered at $f_s/4$ and their bandwidth increases from $f_s/15$ to $f_s/3$ in five equal steps. Figure 3(d) depicts this signal.

5) MPE and IMPE Versus Spectral Content of Colored Noise: In order to investigate the dependence between the MPE or IMPE and the spectral content of colored noise, an autoregressive (AR) process of order 1, $AR(1)$, was generated varying the model parameter, ρ, linearly from +0.9 to –0.9. Its energy therefore moved from low to high frequencies. When ρ was equal to 0, the sequence corresponded to WGN, in the center of the synthetic signal. Figure 3(e) depicts the corresponding spectrogram, time plot and zoom views.

6) MPE and IMPE Versus Changes from being Non-deterministic to Deterministic: In order to inspect how the MPE and IMPE change when a stochastic sequence progressively turns into a periodic deterministic signal. For this end, we generated a MIX process employed by (Pincus 1991, Ferrario, Signorini et al. 2006, Escudero, Hornero et al. 2009) . It is defined as follows:

$$\mathrm{MIX} = (1-z)x + zy \tag{7}$$

where z denotes a random variable which equals 1 with probability p and equals 0 with probability $1-p$, x shows a periodic time-series created by $x_k = \sqrt{2}\sin\left(2\pi k/12\right)$ and y is a uniformly distributed variable on $\left[-\sqrt{3},\sqrt{3}\right]$ (Ferrario, Signorini et al. 2006, Escudero, Hornero et al. 2009). The synthetic time-series was based on a *MIX* process whose parameter varied between 0.01 and 0.99 linearly. Therefore, this signal, depicted in Figure 3(f), evolved from randomness to orderliness.

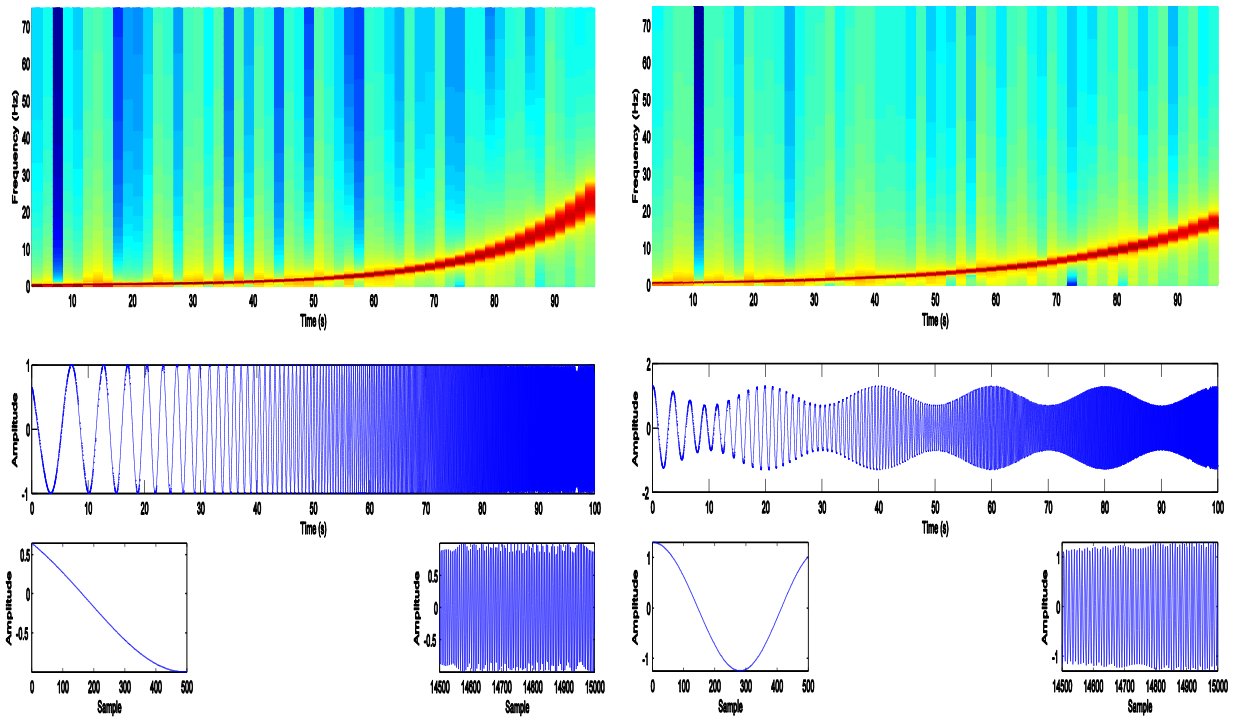

(a) (b)

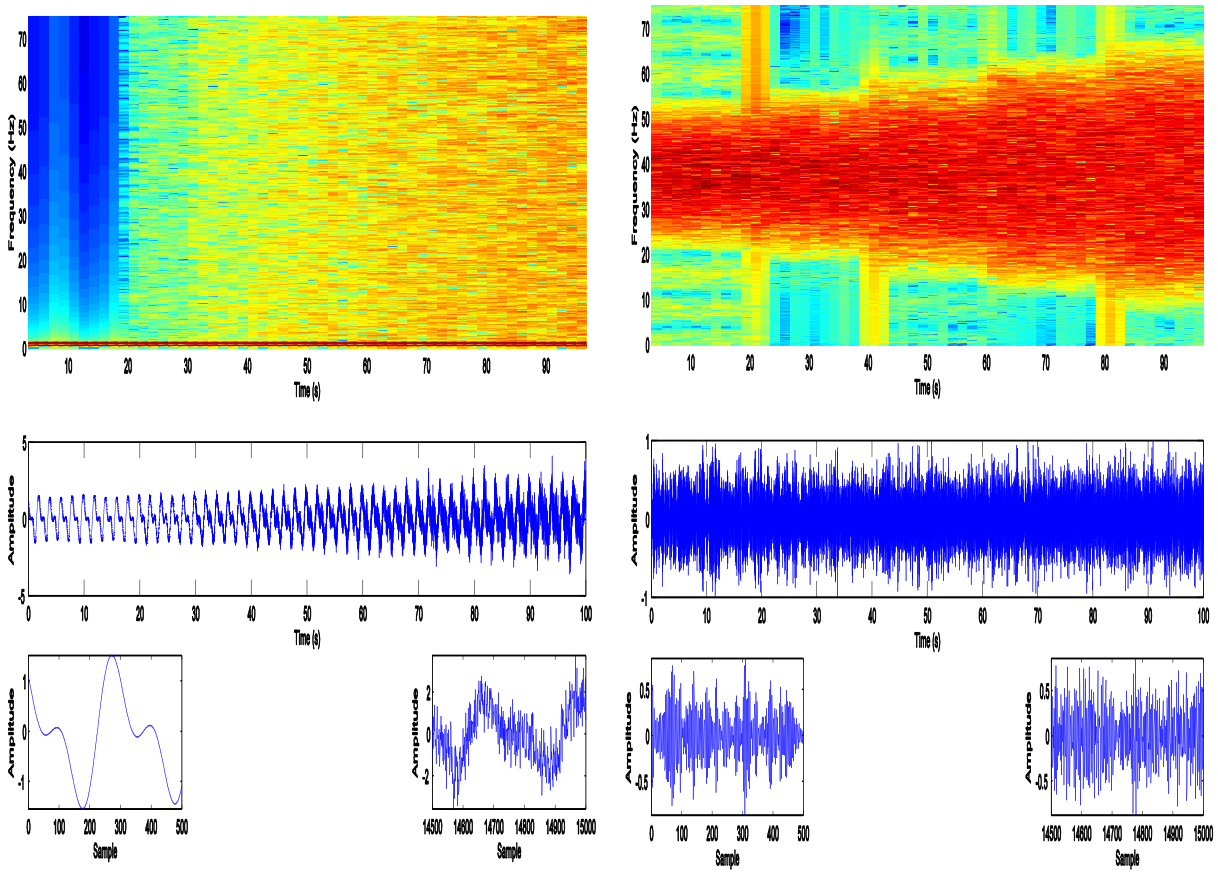

(c) (d)

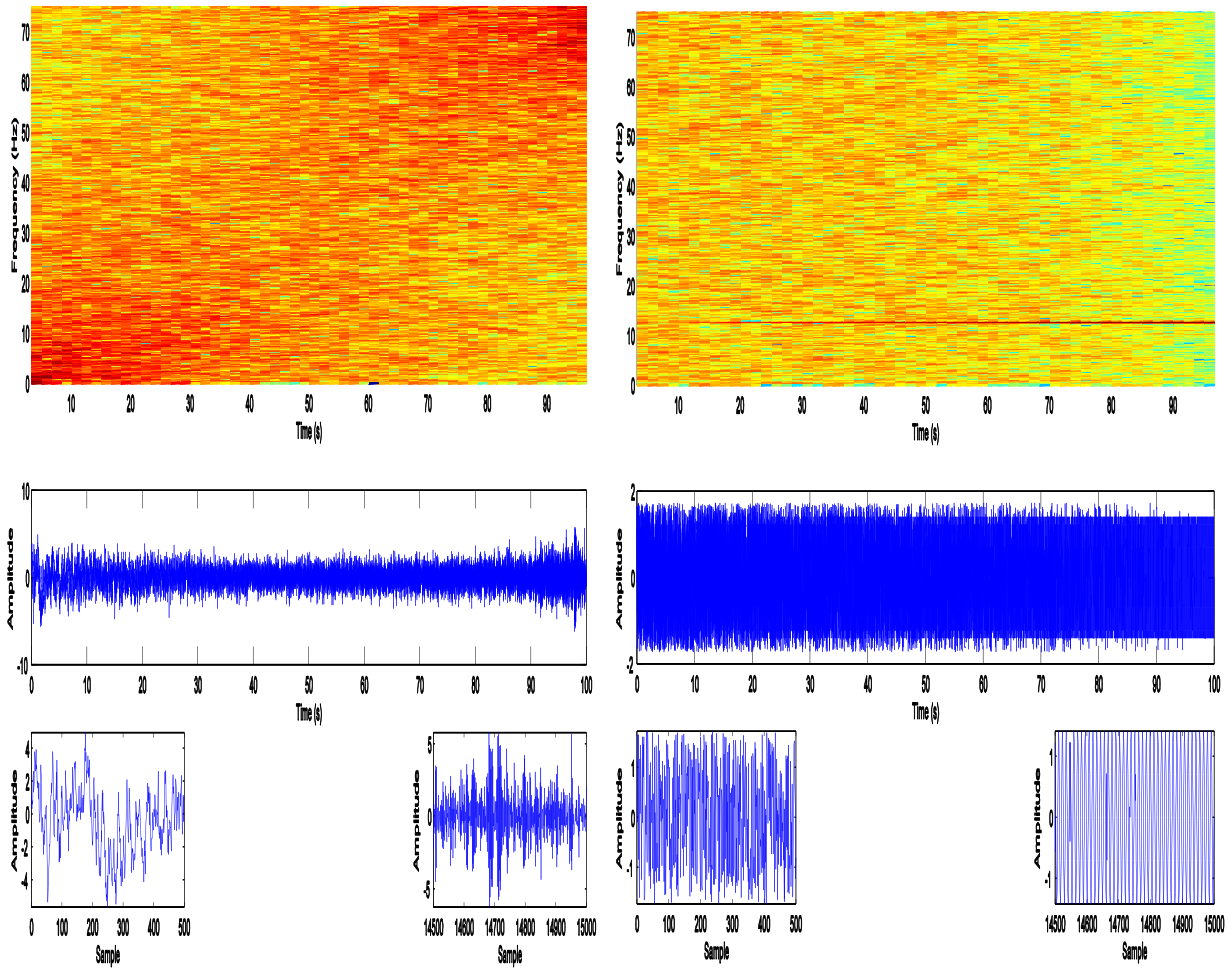

(e) (f)

Figure 3. Spectrograms, time plots and zoom views on the first and last time intervals of the synthetic signals used in this study. (a) Test a: Chirp signal with constant amplitude. (b) Test b: Amplitude modulated chirp signal. (c) Test c: Quasi-periodic signal with increasing additive noise power. (d) Test d: Colored noise with increasing bandwidth. (e) Test e: AR(1) process with variable parameter. (f) MIX process evolving from randomness to periodic oscillations. Red corresponds to high power, and blue corresponds to low power.

4.2. Real EEG signals

The MPE and IMPE were applied to five groups (denoted A, B, C, D, and E) of real EEG signals to compare the ability of each method to account for different characteristics of the real biomedical data. These recordings belong to the EEG database made available online by

Andrzejak et al. at the Department of Epileptology, University of Bonn (Andrzejak, Lehnertz et al. 2001). Here, we only describe these signals briefly and the reader is referred to (Andrzejak, Lehnertz et al. 2001) for additional information. Each of the five datasets consists of 100 single-channel EEG segments of 23.6 s recorded with f_s= 173.61 Hz (4096 sample points).

Subsets A and B include EEG signals recorded extracranially during the relaxed state of five healthy people with eyes closed and eyes open, respectively. The signals in sets A and B were acquired at surface electrodes placed according to the international 10-20 system.

We also applied our methods to three subsets (C, D and E) of EEG data from five epileptic subjects, who had achieved full seizure control after a surgical procedure (Andrzejak, Lehnertz et al. 2001). Therefore, the EEG signals were not acquired in the same way in healthy subjects and epileptic patients.

Signals in set D were recorded from within the epileptogenic zone, whereas segments in set C were acquired from the hippocampal formation of the opposite brain hemisphere. Strip electrodes were implanted onto the lateral and basal regions of the neocortex. Both sets C and D included only activity measured during seizure-free intervals. Nonetheless, it might be possible that some epileptic abnormalities are still present in these recordings. In contrast, set E contains seizure activity throughout (i.e., all epochs in set E were recorded during ictal periods). All EEG recordings were prepared with the same 128-channel amplifier system, employing an average common reference. Electrodes with pathological activity (C, D, and E) or strong eye movement noise (A and B) were removed from the computation of the reference (Andrzejak, Lehnertz et al. 2001).

Before computing the entropy of these signals, all recordings were digitally filtered employing an FIR band-pass filter with cut-off frequencies at 0.5 Hz and 40 Hz, a band typically used in the analyses of brain activity.

5. Results

5.1. Synthetic Signals

In the first place, we evaluated the values of MPE and IMPE for WGN and 1/*f* noise as two widespread sequences in multiscale entropy-based analyses (Costa, Goldberger et al. 2005, Wu, Wu et al. 2013, Wu, Wu et al. 2014).

As it can be seen in Figure 4, for uncorrelated WGN, the MPE and IMPE values decreased monotonically with scale factor τ. This is in agreement with the MSE-based results in (Costa, Goldberger et al. 2005, Wu, Wu et al. 2014). In contrast, for a long-range correlated signal such as 1/*f* noise, the PE values first decreased and then approximately became constant over deeper temporal scales (Figure 5). Each error bar of each scale τ depicts the standard deviation (SD) of the average of results of 40 signals for each WGN or 1/*f* noise. As can be seen in Figures 4 and 5, the results using IMPE had notably smaller SD than those of MPE. The length of the 1/*f* noise and WGN sequences was $N = 20000$. Subsequently $(d+1)! \le \left\lfloor \frac{20000}{40} \right\rfloor = 500$, and d can be given a value of 2, 3 or 4. Here, we chose d=4.

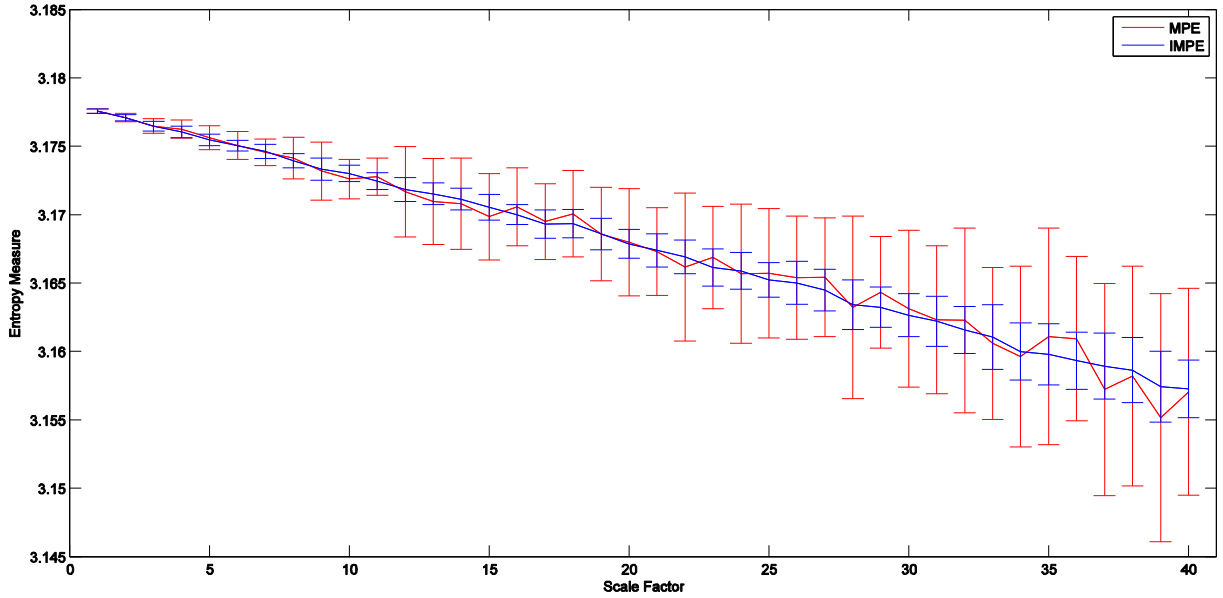

Figure 4. Mean value of results of the MPE and IMPE computed from 40 different WGN test signals. Red and blue indicate MPE and IMPE results, respectively.

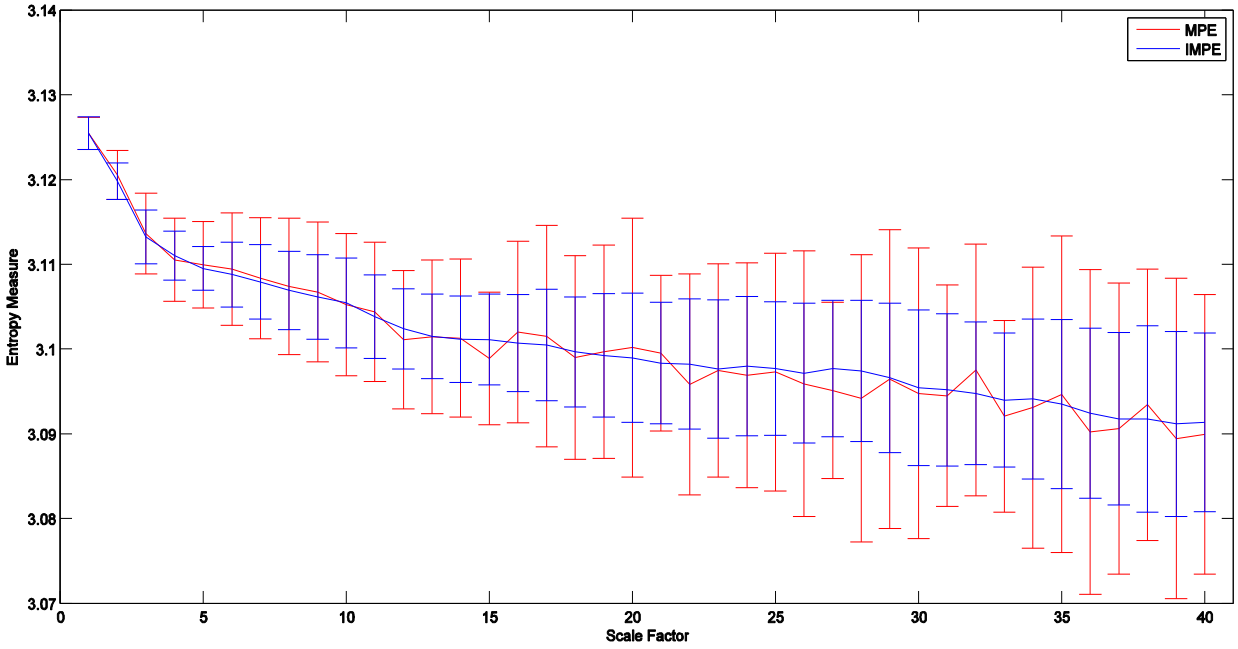

Figure 5. Mean value of results of the MPE and IMPE computed from 40 different 1/*f* noise test signals. Red and blue indicate MPE and IMPE results, respectively.

To understand the relationship between MPE or IMPE and the frequency of a signal, we employed a sliding window moving along a chirp signal. Then, for each scale factor, the MPE or IMPE of that part of the signal was computed. The corresponding results of MPE and IMPE are illustrated in Figures 6(a) and 6(b), respectively. When the window occupied the beginning of the signal, which had lower frequency, the permutation entropy was low. Both the MPE and IMPE increased when considering latter samples of the signal, which were associated with higher frequencies. It can be noticed that, in this case, entropy was maximized when the relationship between temporal window (TW) and scale factor τ was close to: $TW = 0.02315 \cdot \tau^2 - 1.617 \cdot \tau + 80.39$. This curve, which was obtained using a second order polynomial fitting, is shown in the top right part of Figure 6(b). In this case, considering that time is related to the instantaneous frequency of the signal according to $f_i(t) = 0.1 \times 300^{t/100}$ and the relationship between temporal window and time, it is possible to estimate that for some frequencies the coarse-graining process leads to maximal entropy. We also show two additional curves on Figure 6(b), with equations $TW = 0.03216 \cdot \tau^2 - 1.999 \cdot \tau + 76.33$ and $TW = 0.04227 \cdot \tau^2 - 2.381 \cdot \tau + 70.39$, which model similar relationships for which the relationship between frequency of the synthetic signal and scale is such that PE maximises.

To understand the dependence of MPE and IMPE and simultaneous frequency and amplitude of a signal, we used the amplitude modulated chirp signal. The results using MPE and IMPE can be observed in Figures 6(c) and 6(d), respectively. The obtained patterns were very similar to the ones obtained with the constant-amplitude chirp signal.

In Figures 6(e) and 6(f), it can be observed that both the MPE and IMPE were sensitive to changes in additive noise power, becoming larger when noise power increased until they reached saturation. As mentioned in 2.1, the highest possible value of PE for *d*=4 is $\ln(4!) = 3.1781$ as it can be seen in the figures. We have also shown the curve in Figure 6(f) that approximately limits the range of maximal entropy. This is given by $TW = 0.281 \cdot \tau^2 + 1.98 \cdot \tau + 9.159$.

Figures 6(g) and 6(h), respectively, show the relationship between MPE or IMPE and the bandwidth of noise. In case of $\tau = 1$ or $\tau = 2$, the PEs gradually increased along the signal. This fact is due to the increasing bandwidth of the noise. From $\tau = 3$ to $\tau = 30$, the PE values is decreasing slowly, while in each scale factor, PEs are relatively equal.

The results demonstrated in Figures 6(i) and 6(j) represent how the MPE and IMPE, in that order, change with the signal spectral content investigated using an AR process. For smaller scale factors, the PEs increase until almost the middle of the signal and then decrease. As can be seen in Figures 6(i) and 6(j), the general trend of the PEs is decreasing from $\tau = 1$ to $\tau = 30$.

Figure 6(k) and Figure 6(l), respectively, show the results of MPE and IMPE using the test signal which aimed to model the evolution from randomness to deterministic oscillations. The frequency of the MIX signal at the latter samples was 1/12. Hence, high PE values can be observed for the temporal scales $\tau = \frac{1}{f} = 12$ and its multiple, $\tau = 24$. The curves that seem to approximate limit the ranges of maximal entropy are also shown in Figure 6(l) as $TW = 0.7712 \cdot \tau^2 + 18.63 \cdot \tau - 43.79$ and $TW = -0.6916 \cdot \tau^2 + 33.42 \cdot \tau - 334.9$, respectively

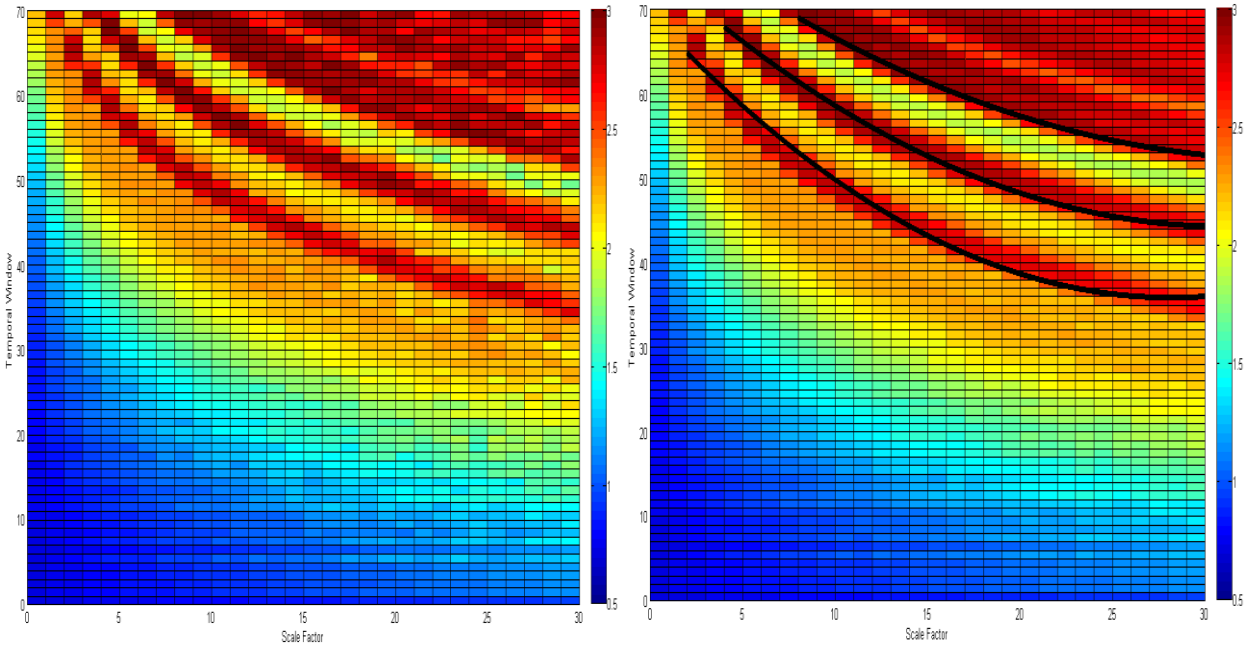
Temporal Window
Scale Factor
Temporal Window
Scale Factor

(a) (b)

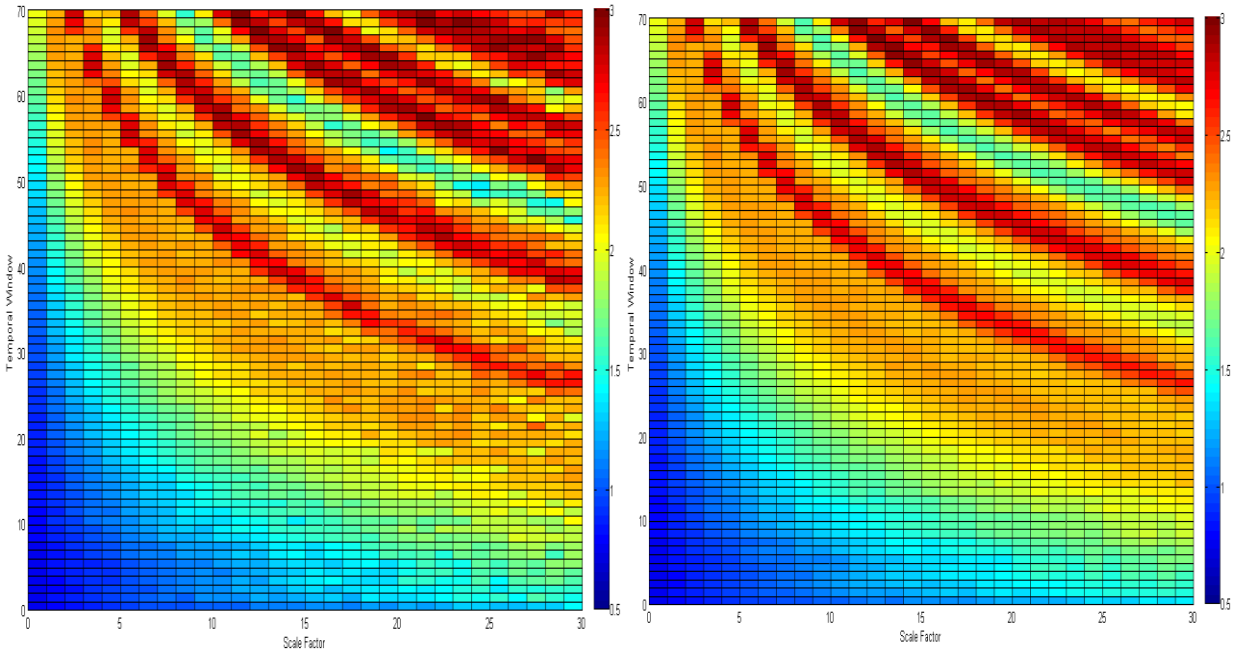
Temporal Window
Scale Factor
Temporal Window
Scale Factor

(c) (d)

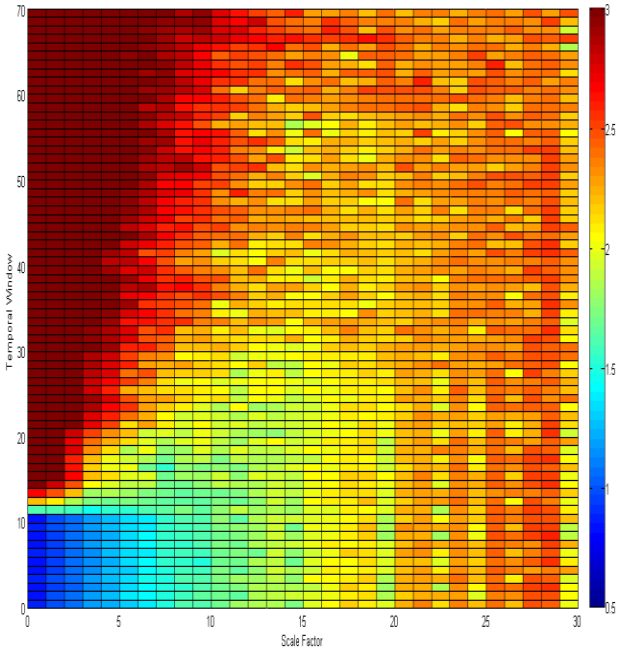
Temporal Window
Scale Factor

(e)

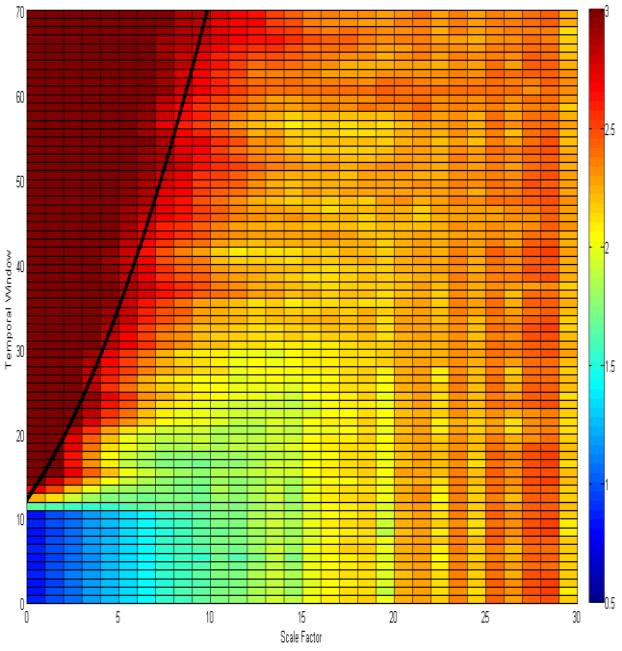
Temporal Window
Scale Factor

(f)

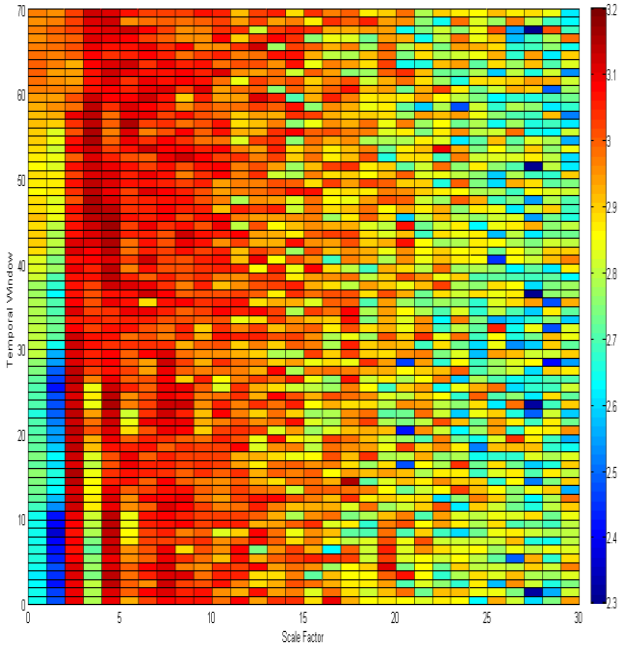
Temporal Window
Scale Factor

(g)

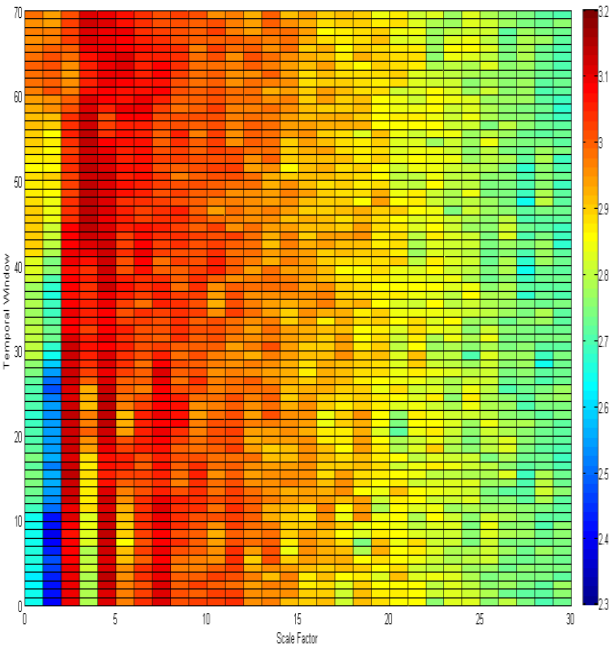
Temporal Window
Scale Factor

(h)

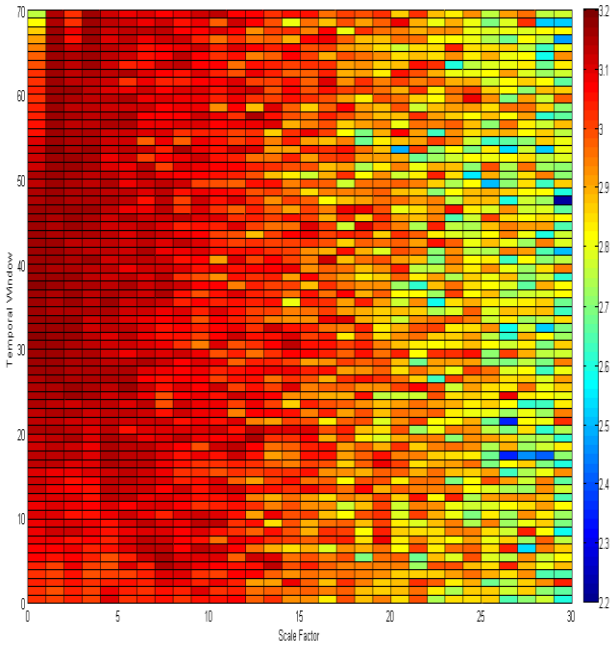
Temporal Window
Scale Factor

(i)

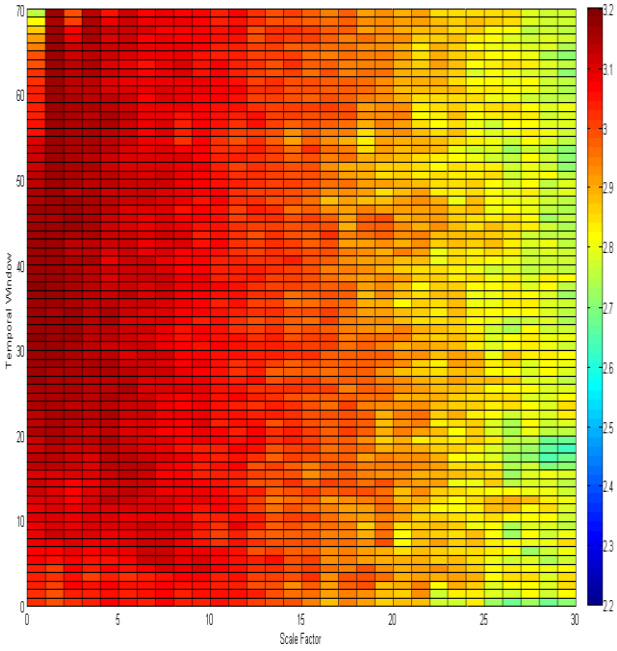
Temporal Window
Scale Factor

(j)

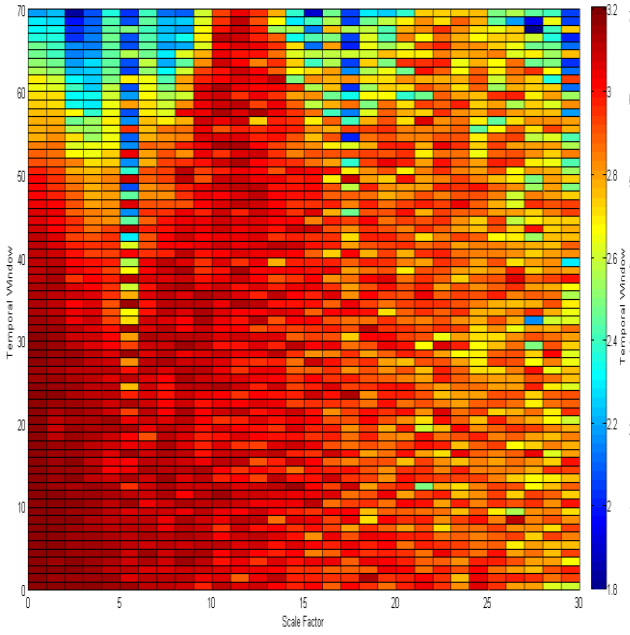
Temporal Window
Scale Factor

(k)

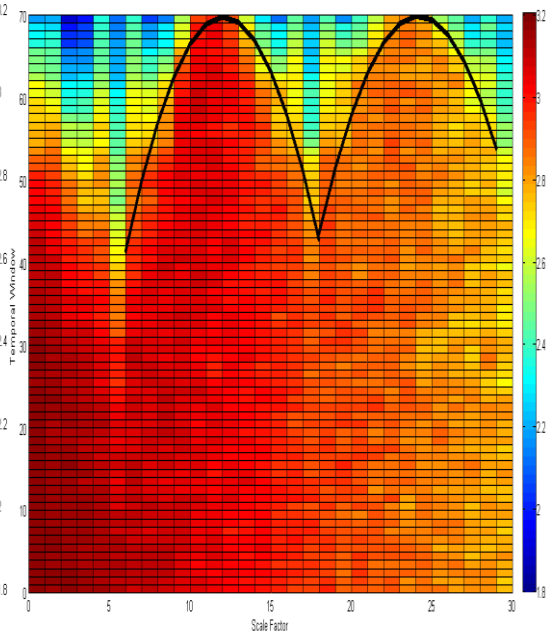
Temporal Window
Scale Factor

(l)

Figure 6. Results of the tests performed to gain better understanding MPE and its interpretation. Relationships between: (a) MPE and chirp signal with constant amplitude, (b) IMPE and chirp signal with constant amplitude, (c) MPE and amplitude-modulated chirp signal, (d) IMPE and amplitude-modulated chirp signal, (e) MPE and quasi-periodic signal with increasing additive noise power, (f) IMPE and quasi-periodic signal with increasing additive noise power, (g) MPE and a signal including five segments of colored noise with increasing bandwidth, (h) IMPE and a signal including five segments of colored noise with increasing bandwidth, (i) MPE and AR(1) process with variable parameter, (j) IMPE and AR(1) process with variable parameter, (k) MPE and a MIX process which evolves from randomness to periodic oscillations, (l) IMPE and a MIX process which evolves from randomness to periodic oscillations.

We also compared some of these results with the MMPE approach by (Shaobo, Kehui et al. 2014) . The performance of the MMPE method, which subsamples the original signal without any averaging or filtering, is shown for the chirp signal with constant amplitude and a quasi-periodic signal with increasing additive noise power in Figures 7(a) and 7(b), respectively. Comparing these figures with the corresponding results of IMPE (Figures 6(b) and 6(f), respectively), it can be appreciated the difference in the entropy results. In addition to the abovementioned technical problems of MMPE, MMPE may not able to characterize the constant chirp time series and quasi-periodic signal with increasing additive noise power in the larger scale factors τ.

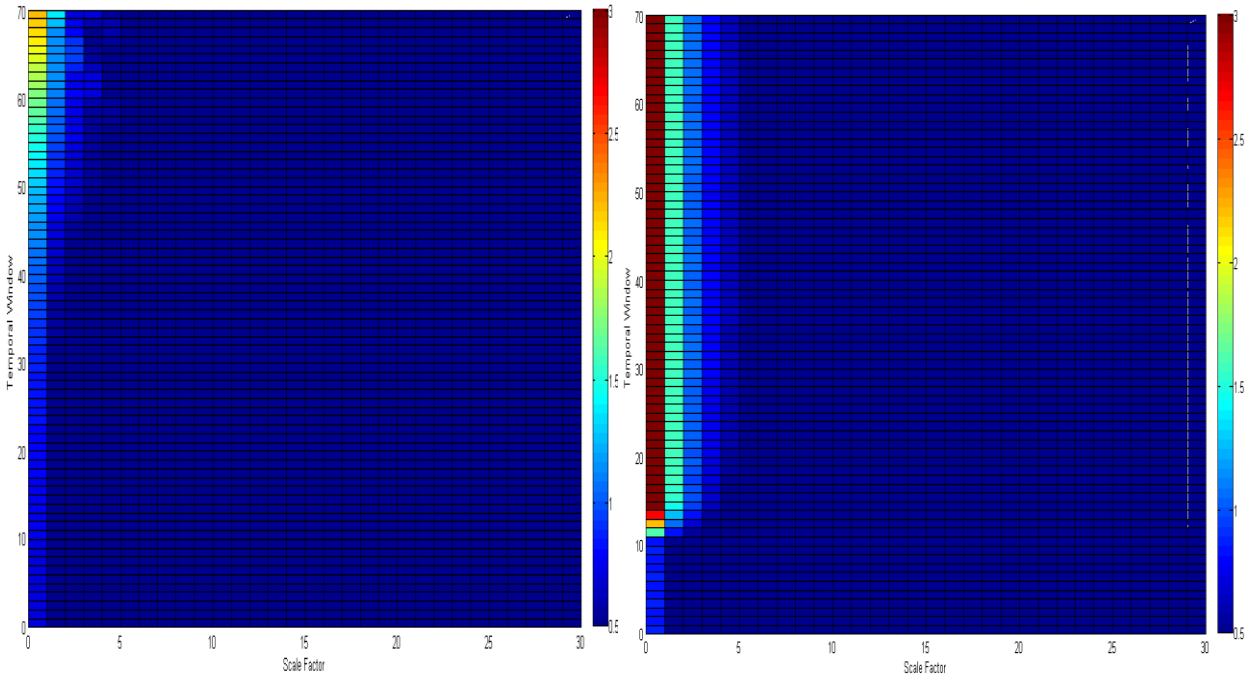

(a) (b)

Figure 7. Results of the tests performed using MMPE (Shaobo, Kehui et al. 2014). (a) Relationship between MMPE and chirp signal with constant amplitude, and (b) MMPE and quasi-periodic signal with increasing additive noise power.

5.2. Real EEG Signals

We illustrate the performance of the IMPE and MPE to characterize real EEG signals using datasets A, B, C, D, and E. Each of them includes 100 signals with a length of 4097 sample points. Since $(d+1)! \le \left\lfloor \frac{4097}{30} \right\rfloor = 136$, d can be equaled 2, 3, or 4.

For *d*=2, *d*=3 and *d*=4, the results for the MPE and IMPE of sets A, B, C, D, and E are shown in Figures 8, 9 and 10, respectively. The error bar of each scale τ demonstrates the SD of the mean value of results of 100 signals for each real

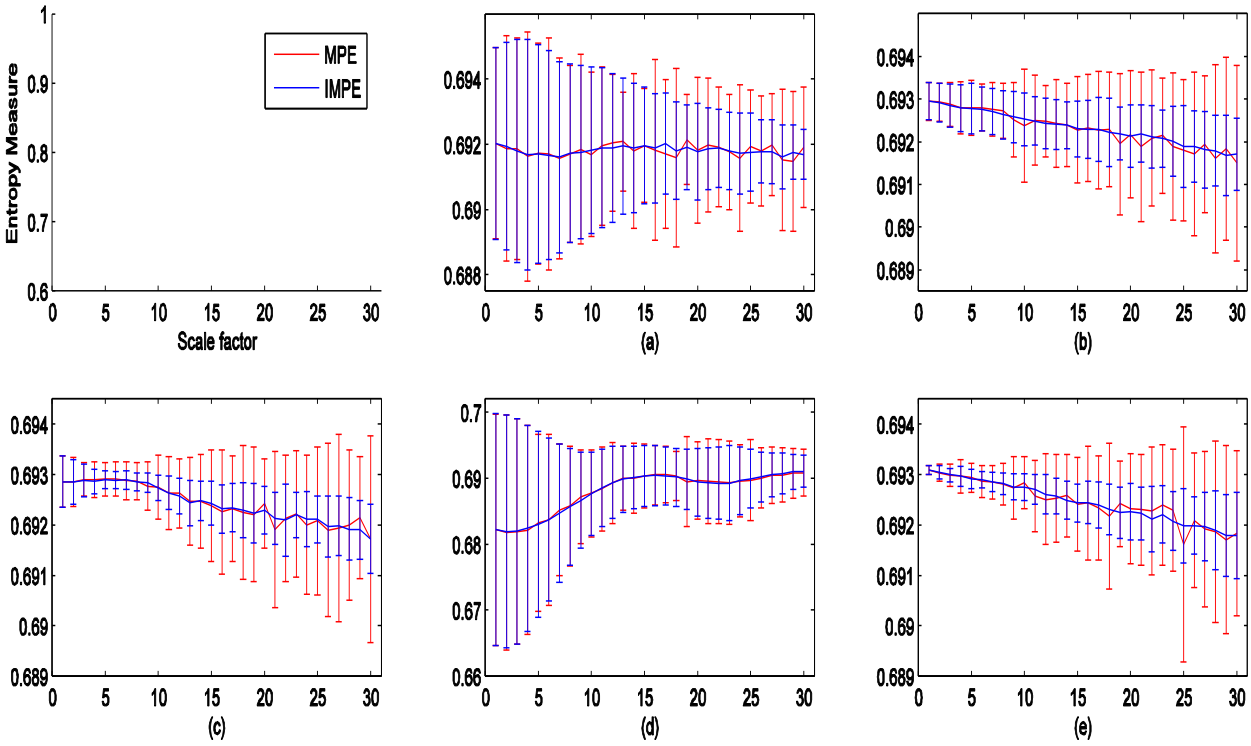

Figure 8. Plots with error bars illustrating the distributions of the permutation entropy values computed from real EEG signals (embedding dimension *d*=2). (a) Surface EEG signals recorded from healthy volunteers with eyes open. (b) Surface EEG signals recorded from healthy volunteers with eyes closed. (c) EEG signals recorded from epilepsy patients in the hippocampal formation of the opposite hemisphere of the brain. (d) EEG signals recorded from epilepsy patients in the epileptogenic zone during a seizure-free interval. (e) EEG signals recorded from epilepsy patients during epileptic seizures.

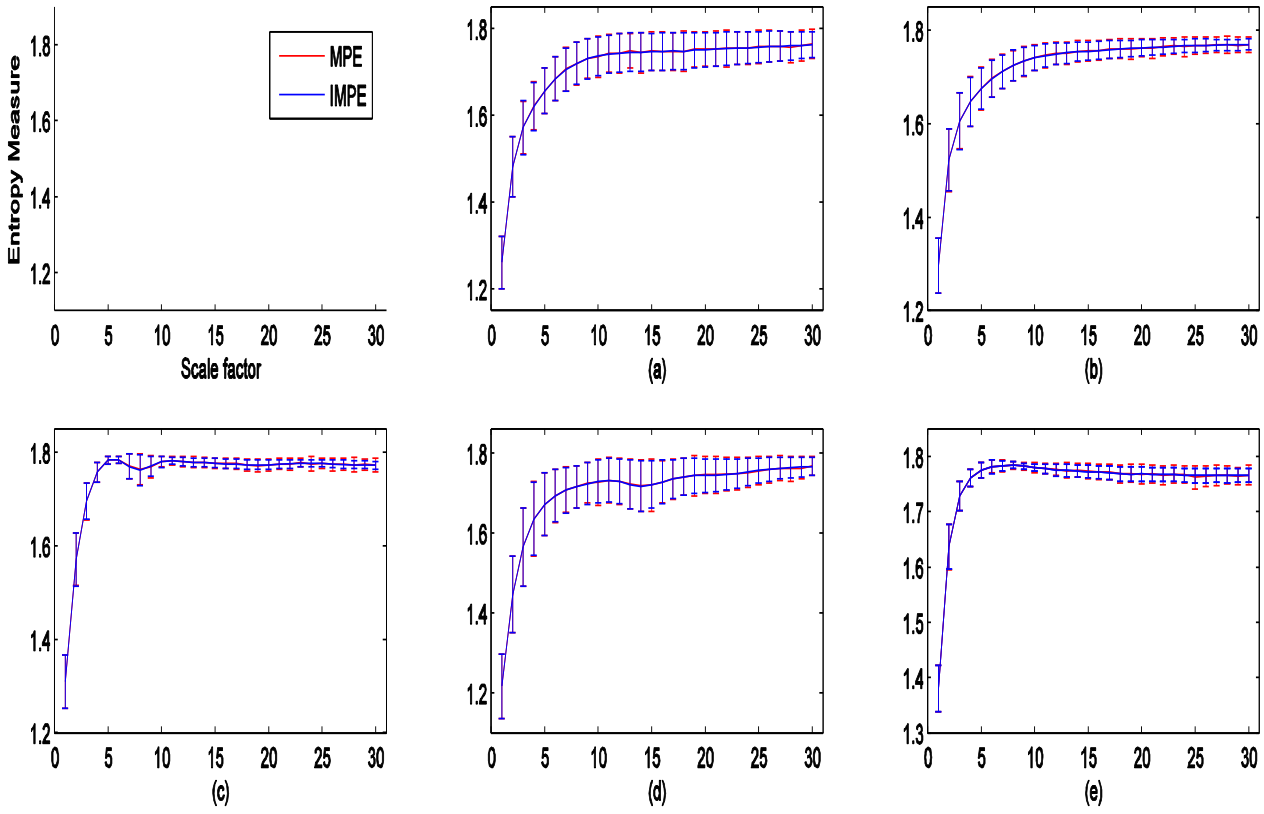

Figure 9. Error bars illustrating the distributions of the permutation entropy values computed from real EEG signals (embedding dimension d=3). (a) Surface EEG signals recorded from healthy volunteers with eyes open. (b) Surface EEG signals recorded from healthy volunteers with eyes closed. (c) EEG signals recorded from epilepsy patients in the hippocampal formation of the opposite hemisphere of the brain. (d) EEG signals recorded from epilepsy patients in the epileptogenic zone during a seizure-free interval. (e) EEG signals recorded from epilepsy patients during epileptic seizures.

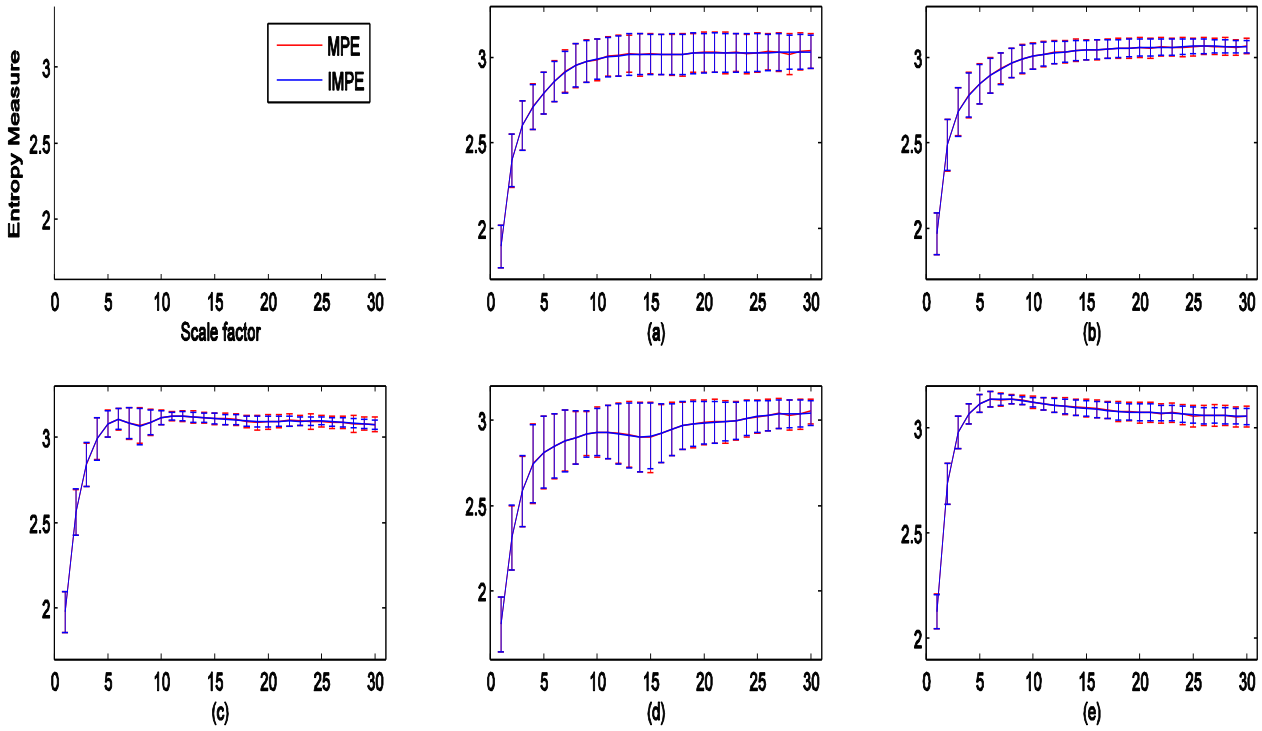

Figure 10. Error bars illustrating the distributions of the permutation entropy values computed from real EEG signals (embedding dimension d=4). (a) Surface EEG signals recorded from healthy volunteers with eyes open. (b) Surface EEG signals recorded from healthy volunteers with eyes closed. (c) EEG signals recorded from epilepsy patients in the hippocampal formation of the opposite hemisphere of the brain. (d) EEG signals recorded from epilepsy patients in the epileptogenic zone during a seizure-free interval. (e) EEG signals recorded from epilepsy patients during epileptic seizures.

6. Discussions

In this study, the behavior of MPE and IMPE for synthetic signals, in terms of straightforward signal processing concepts, and real EEG data was assessed.

6.1. Synthetic Signals

The comparison of $1/f$ noise and WGN illustrated that $1/f$ noise is structurally more complex than uncorrelated WGN. It is also important to notice that the mean values of MPE and IMPE for all scale factors were approximately equal, although the estimations of entropy based on IMPE had smaller variability than those of MPE. In other words, the SD of each of entropy measure using IMPE for each scale factor was smaller than the SD of corresponding ones using MPE. This fact confirms our theoretical expectations about IMPE producing more stable results than MPE.

For both the constant and amplitude modulated chirp signal, the values of PE tended to increase as the temporal window progressed along the signal, until they reach a plateau of high values. For these signals, the PE values provided by the IMPE were more robust and stable than those obtained by the MPE. Moreover, for both synthetic signals, the IMPE values changed more smoothly than the MPE ones at all scales when moving from the first to the last samples. Another important point is that the comparison of results obtained by using the constant and amplitude modulated chirp signals showed the PE values do not significantly change with slow changes in amplitude.

In the case of the quasi-periodic synthetic signal, the PE values in the deeper temporal windows for both the MPE and IMPE generally increase. In addition, the fluctuations between two successive scale factors or temporal windows were smaller for IMPE than for MPE. As can be seen in Figure 6(e), when we focus on the scale factor 1 (τ=1, i.e., original PE), the amount of noise power is not recognizable from the entropy values because they have saturated. However, when considering deeper scale factors, it is possible to appreciate that different levels of noise power led to a different number of temporal scales being saturated. This depicts the importance of multiscale concept in signal processing applications.

For colored noise with increasing bandwidth, when the scale factor τ was too high, the effective sampling frequency of the coarse-graining sequence became very low, and such effective sampling frequency might be below the lower limit of the bandwidth of the colored noise (because our colored noise is centered at $f_s/4$). In this case, both MPE and IMPE behaved similarly because their entropy values decrease, although the results provided by IMPE are still more stable than those of MPE.

This analysis on AR(1) process with variable parameter showed that part of the signal with wider spectra (e.g., white noise) provides higher PEs. In contrast, time series with narrower spectral content produces lower PEs, regardless of whether their spectra were centered at low or high frequencies. When the scale factor τ goes up, the general pattern for both MPE and IMPE decreased gradually.

As expected on the basis of the concept of entropy, moving along the mix process evolving from randomness to periodic oscillations, the PEs decreased for both of MPE and IMPE, although for IMPE, the change was more stable. In addition, the highest scale factors lead to lower values of entropy for both the IMPE and MPE. Nonetheless, if a signal has one single frequency component, then the temporal scales where τ equals the period of that component will lead to a coarse-graining sequence that has almost no signal contribution, as this will have been averaged out. In such case, any small presence of noise may lead to high values of entropy, as evidenced by the maximal values of entropy for τ=12 and τ=24 in Figure 6(l).

6.2. Real EEG Signals

The mean values of MPE and IMPE for all scale factors and sets were approximately equal, although the averages of IMPE results were comparatively more stable. Moreover, for almost all

scale factors changing from 1 to 30, each SD of results of IMPE was smaller than the corresponding SD of results of MPE. This fact hence confirms the superiority of IMPE over MPE in terms of stability of the results.

It should be added that the intracranial EEG signals' amplitudes are around 100 mV, while those of seizure activity voltages can exceed 1000 mV. However, different levels of amplitude do not affect the outcomes of the PE considerably because this entropy measure is sensitive to the frequencies and the ordering of the samples, instead of the amplitudes, of the signals.

In addition to the interpretation of MPE and IMPE in terms of the changes in frequency, bandwidth, amplitude, and power noise depicted with the synthetic signals; our results illustrated that both the MPE and IMPE can be employed as a powerful indicator of complexity in biomedical signals. Hence, MPE and IMPE may be used to distinguish disorders and irregularities of physiological recordings.

All in all, although the ranges of the results for both MPE and IMPE are similar, the variability of IMPE for subsequent temporal scales is smaller than MPE. This is because, for each scale, the standard deviation of IMPE results are notably smaller than MPE results on the synthetic data and real biomedical signals. This fact is because of averaging the results of several new proposed versions of the coarse-grained sequences. Hence, IMPE may be better able to characterize abnormal dynamics related to disease.

7. Conclusions

MPE is a powerful indicator of entropy for different types of signals, including nonlinear and non-stationary signals. To increase the stability of MPE, we have proposed the IMPE. Then,

using synthetic signals, the MPE and IMPE results were investigated to better understand their behavior in terms of signal processing concepts such as frequency, amplitude, noise power, and signal bandwidth. The results showed that a signal with noise, larger bandwidth and/or higher frequency would generally lead to higher values of entropy. MPE and IMPE results were not sensitive to slow changes in amplitude. In the deeper scale factors, because of the filtering effect of the coarse-graining process, the MPE and IMPE tended to have lower values for the tested signals, except for constant and amplitude modulated chirp signals. Furthermore, the capabilities of MPE and IMPE to assess physiological complexity were assessed by analyzing publicly available EEG signals. The results derived from both synthetic and real EEG signals support the idea that IMPE has a better performance than MPE, although both are useful and informative tools to calculate the complexity of a time series.

Acknowledgments

The authors would like to thank Dr. Andrzejak from the Department of Information and Communication Technologies, Universitat Pompeu Fabra, Barcelona, Spain, for providing the EEG data described in Section 4. They also want to thank the editor and the reviewers for fruitful comments and suggestions.

References

Primary Sources

Secondary Sources

Uncategorized References

Andrzejak, R. G., et al. (2001). "Indications of nonlinear deterministic and finite-dimensional structures in time series of brain electrical activity: Dependence on recording region and brain state." PHYSICAL REVIEW E **64**(6): 1-8.

Bandt, C. and B. Pompe (2002). "Permutation Entropy: A Natural Complexity Measure for Time Series." Physical Review Letters **88**(17): 1-4.

Costa, M., et al. (2002). "Multiscale Entropy Analysis of Complex Physiologic Time Series." Physical Review Letters **89**(6): 1-4.

Costa, M., et al. (2005). "Multiscale entropy analysis of biological signals." PHYSICAL REVIEW E **71**(2): 021906.

Diebold, F. (2006). Elements of forecasting, Cengage Learning.

Escudero, J., et al. (2009). "Interpretation of the auto-mutual information rate of decrease in the context of biomedical signal analysis. Application to electroencephalogram recordings." Physiological measurement **30**(2): 187.

Ferlazzo, E., et al. (2014). "Permutation entropy of scalp EEG: A tool to investigate epilepsies: Suggestions from absence epilepsies." Clinical Neurophysiology **125**(1): 13-20.

Ferrario, M., et al. (2006). "Comparison of entropy-based regularity estimators: application to the fetal heart rate signal for the identification of fetal distress." Biomedical Engineering, IEEE Transactions on **53**(1): 119-125.

Fogedby, H. (1992). "On the phase space approach to complexity." Journal of Statistical Physics **69**(1-2): 411-425.

Goldberger, A. L., et al. (2002). "What is physiologic complexity and how does it change with aging and disease?" Neurobiology of Aging **23**(1): 23-26.

Holzinger, A., et al. (2014). On Entropy-Based Data Mining. Interactive Knowledge Discovery and Data Mining in Biomedical Informatics. A. Holzinger and I. Jurisica, Springer Berlin Heidelberg. **8401:** 209-226.

Kantz, H., et al. (2011). Nonlinear analysis of physiological data, Springer Publishing Company, Incorporated.

Kowalski, A., et al. (2007). "Bandt–Pompe approach to the classical-quantum transition." Physica D: Nonlinear Phenomena **233**(1): 21-31.

Li, J., et al. (2014). "Using Permutation Entropy to Measure the Changes in EEG Signals During Absence Seizures." Entropy **16**(6): 3049-3061.

Li, X., et al. (2007). "Predictability analysis of absence seizures with permutation entropy." Epilepsy Research **77**(1): 70-74.

Morabito, F. C., et al. (2012). "Multivariate multi-scale permutation entropy for complexity analysis of Alzheimer's disease EEG." Entropy **14**(7): 1186-1202.

Pincus, S. M. (1991). "Approximate entropy as a measure of system complexity." Proceedings of the National Academy of Sciences **88**(6): 2297-2301.

Sanei, S. (2013). Adaptive Processing of Brain Signals, John Wiley & Sons.

Sejdić, E. and L. A. Lipsitz (2013). "Necessity of noise in physiology and medicine." Computer Methods and Programs in Biomedicine **111**(2): 459-470.

Shaobo, H., et al. (2014). "Modified multiscale permutation entropy algorithm and its application for multiscroll chaotic systems." Complexity.

Wu, S.-D., et al. (2013). "Modified multiscale entropy for short-term time series analysis." Physica A: Statistical Mechanics and its Applications **392**(23): 5865-5873.

Wu, S.-D., et al. (2014). "Analysis of complex time series using refined composite multiscale entropy." Physics Letters A **378**(20): 1369-1374.

Zanin, M., et al. (2012). "Permutation Entropy and Its Main Biomedical and Econophysics Applications: A Review." Entropy **14**(8): 1553-1577.

Appendix

The codes of synthetic signals and IMPE are available online at http://dx.doi.org/10.7488/ds/273.